


Dynamic Recrystallization and Dynamic Precipitation in AA6061 Aluminum Alloy During Friction Stir Welding

Wang Tao¹  · Duan Shuwei² · Kenji Matsuda³ · Zou Yong²

Received: 2 October 2021 / Accepted: 26 November 2021 / Published online: 27 January 2022
© The Indian Institute of Metals - IIM 2021

Abstract This paper investigated the mode of recrystallization in the nugget zone (NZ) of friction stir welding (FSW) joint of AA6061-T6. By correlating grain orientation spread results, kernel average misorientation (KAM) results, misorientation maps of grain boundaries (GBs) and selected area diffraction patterns of precipitates systematically, we found that continuous dynamic recrystallization (CDRX) and geometric dynamic recrystallization (GDRX) both occurred. CDRX could be enhanced by decreasing feeding speed of FSW. The variation trend of fraction of low-angle grain boundaries in NZ indicated different contribution brought by CDRX and GDRX and also different combination form of heat input. KAM results can also act as indicator of the extent of dynamic recrystallization in the NZ of FSW, only under a constant feeding speed. The fine needle-shaped β'' precipitate disappeared in NZ and evolved to β' and equilibrium β -Mg₂Si phase during FSW. Furthermore, the shape and orientation of β' or β phases could be changed by mutual interaction with dislocation movement, to different extent depended on CDRX.

Keywords Friction stir welding · Grain orientation spread · Dynamic recrystallization · Transmission electronic microscopy

1 Introduction

With the aid of high-resolution electron backscattered diffraction, grain orientation spread (GOS) and kernel average misorientation (KAM) maps are more and more applied to analysis of deformation degree of Al alloy [1–4]. The final Al alloy products can be obtained via a variety of thermal–mechanical processings. During these operations, friction stir welding (FSW) [5, 6] exerts high temperature (typically > 0.5 T_m) [7] and severe plastic deformation to the joint instantaneously. Thus, different from static recrystallization followed by cold deformation and annealing treatment, dynamic recrystallization has been reported to exist in NZ during FSW [8].

Welding parameters, including rotation speed, feeding speed, shoulder diameter of the tool, pin shape and axial force, will influence the microstructure of the joint, especially NZ, according to recent studies using response surface methodology [9, 10]. When studying FSW of AA7075 with high strength, Bisadi [11] found that shoulder diameter of the tool had considerable effects on the heat input, compared to the pin shape; meanwhile, the pin shape had considerable effects on the plastic deformation. It results in distinct variations of metal flow mode within the NZ (one mode near the shoulder and the other one mode around the pin) [12]. For some non-heat-treatable Al alloy with a moderate strength [13], fine and fragmented dynamically recrystallized grains form in nugget zone (NZ), with tensile fracture outside NZ and strength equal to about 90% of the base metal. AA6061 Al–Mg–Si–(Cu) alloy is widely used

✉ Zou Yong
yzou@sdu.edu.cn

¹ School of Materials Science and Engineering, Shandong University, Jinan 250061, China

² MOE Key Lab of Liquid-Solid Structure Evolution and Materials Processing, Institute of Materials Joining, Shandong University, Jinan 250061, China

³ Department of Materials Science and Technology, Faculty of Engineering, University of Toyama, Toyama 930-8555, Japan

in transportation industries. As a heat-treatable Al–Mg–Si alloy with a moderate strength, on the one hand, it is easy to get fine and fragmented dynamically recrystallized grains. On the other hand, the dynamical recrystallization character seems different from high-strength heat-treatable Al alloy, according to EBSD studies on metal flow transfer in dissimilar FSW joint between AA6082-T6 and AA2014-T6 [14], or between dissimilar FSW joint of AA6082-T6 and AA7075-T651 [12].

In this paper, we focus on the effects of rotation speed and feeding speed on recrystallization characteristics of FSW joint by using GOS and KAM, which were rarely done, especially for moderate-strength aging-hardening Al–Mg–Si alloy. For AA6061, it contains various strengthening precipitates such as the GP-I zones, GP-II zones (β''), β' and β . Since dislocation substructures play a key role in recrystallization [2], the interaction between small precipitates and dislocation is also critical to control the grain structure [15]. By studying the evolution of micro-substructure and precipitates, we aim to reveal the effect of FSW parameters, especially rotation speed and feeding speed, on the mode of dynamic recrystallization and the feature of phase transformation.

2 Experimental Procedure

The AA6061-T6 plates of 5.85 mm thick, with tensile strength $R_m \approx 306$ MPa and tensile elongation $\delta \approx 14\%$ as shown in Fig. 1, were butt-welded using an FSW machine (FSW-3LM-3012). The chemical composition is shown in Table 1. The welding tool is schematically illustrated in Fig. 2. It comprises a shoulder with two concentric grooves and a conical pin with 5.54 mm length and 5 mm diameter at half-length. The screw of tool pin is

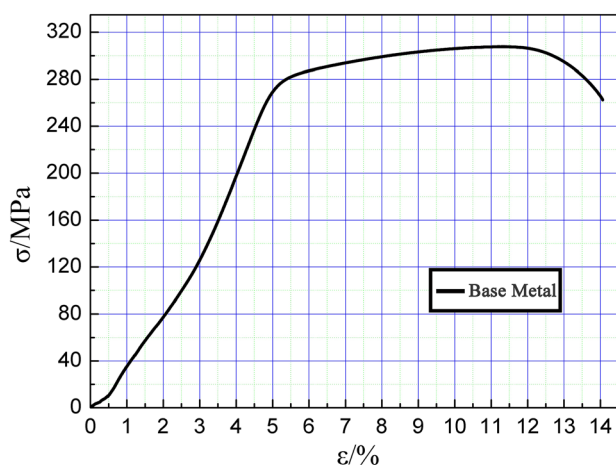


Fig. 1 The engineering stress–strain curves of tensile tests for 6061-T6 base metal

Table 1 Chemical composition of AA6061-T6 (mass%)

Si	Fe	Cu	Mn	Mg	Cr	Ti	Zn	Al
0.574	0.350	0.199	0.038	0.991	0.120	0.024	0.016	Bal

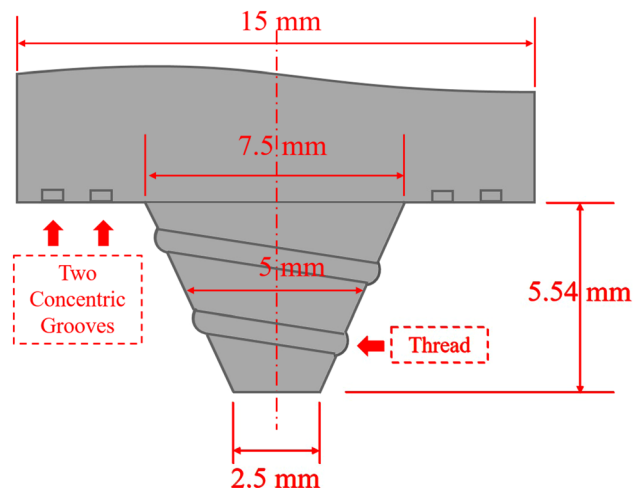


Fig. 2 The schematic representation (with dimensions) of the welding tool

left-threaded around the cone to generate the down forging force. The back tilting angle of the tool is 2.5° during FSW. FSW trials were carried out at a feeding speed from 60 to 250 mm/min (millimeter per minute) for various rotation speeds. The welded pieces were cooled in air after welding.

We used a JSM-7800F scanning electron microscope (SEM) (Tokyo, Japan) and Oxford NordlysMax3 system to acquire electron backscattered diffraction (EBSD) data and then processed them with Channel 5 commercial software (v5.12.67.0). The EBSD images were observed on the transverse cross section perpendicular to the welding direction and at the mid-thickness position of the center area in the NZ. The GOS was calculated for each scan. GOS maps were determined by the degree of orientation change between every pixel in the grain and the grain average orientation within a grain, where 15° or higher misorientation was used to define a grain boundary. The grain was then colored by the average measurement for all of its constituent pixels. It is a classification of whole grains, which acts as a primary strain analysis tool revealing grains which show the most deformation. KAM maps were also obtained by Local Misorientation Component of Channel 5 software. KAM, which indicates deformation extent, represents the average misorientation (within 5°) of each pixel with respect to its surrounding pixels and assigns the mean value to that pixel. Misorientations over a certain value are also discarded, so that the misorientations associated with discrete subgrain and grain

boundaries are excluded. TEM samples were prepared by Twin Jet Thinning instrument. The foil specimens from the NZ were sliced for TEM observation in a Topcon EM-002B transmission electron microscope.

3 Experimental Results

The welding parameters for all the trials are listed in Fig. 3 with macrographs of transverse section of joints. All of them have no obvious welding defects. The grain size of NZ in FSW joint is only a few microns seen from Fig. 4, which is much smaller than that in matrix because of dynamic recovery and dynamic recrystallization [16–18]. There exist 3 styles of dynamic recrystallization [19, 20]: (1) discontinuous dynamic recrystallization (DDRX), which occurs in alloys with low stacking fault energy by nucleation and growth of new grains; (2) continuous dynamic recrystallization (CDRX), which involves the formation of arrays of low-angle boundaries and a gradual increase in the boundary misorientation during hot deformation, finally leading to new grain development; (3) geometric dynamic recrystallization (GDRX), resulting from the impingement of serrated grain boundaries which can occur when grains are extremely elongated by severe hot deformation. For AA6061 that has a high layer fault energy [21, 22], CDRX and GDRX mainly occur concomitantly [23, 24]. Meanwhile, it seems difficult to distinguish the mode of dynamic recrystallization, as a dislocation net can be seen within a grain, regardless of welding parameters.

In order to see more clearly, a larger area containing several adjacent grains was observed. As it is shown in Fig. 5, the grains A, B and C seem formed from an elongated grain according to their similar orientation and width. Because the orientation of the $[110]_{Al}$ selected area diffraction patterns obtained by adjusting the angle of the double tilt sample holder is consistent, the misorientation θ can be calculated directly by the formula (1) [25]:

$$\cos \theta = \cos \Delta\alpha \cos \Delta\beta + 2 \sin \alpha_1 \sin \alpha_2 \sin \left(\frac{\beta_2 - \beta_1}{2} \right)^2 \tag{1}$$

$$\Delta\alpha = \alpha_2 - \alpha_1 \tag{2}$$

$$\Delta\beta = \beta_2 - \beta_1 \tag{3}$$

where α is tilt angle of X axis and β is tilt angle of Y axis. Then, the calculated misorientation between grains A and C is 8.76° , which belongs to low-angle grain boundary. The grain B was wedged into the grain boundary between grains A and C. The misorientation of grain A–B and B–C is 7.16° and 1.40° , respectively. Although low-angle grain boundary (LAGB) can be confirmed according to the definition ($2^\circ < \text{LAGB} < 15^\circ$), the formation mechanism of these LAGBs is different. It is easy to find that the dislocation density in grain B is obviously lower than that in A and C. The misorientation of the sub-grain boundary cannot increase continuously by consuming dislocations. Even with the increase in strain or at a very high temperature ($< 0.9 T_m$, T_m is the melting point), the orientation difference of subgrain boundary is still stable at a very low angle ($< 4^\circ$) [26]. The increment formula of

Fig. 3 Macrographs of transverse section for FSW joints obtained at various welding parameters

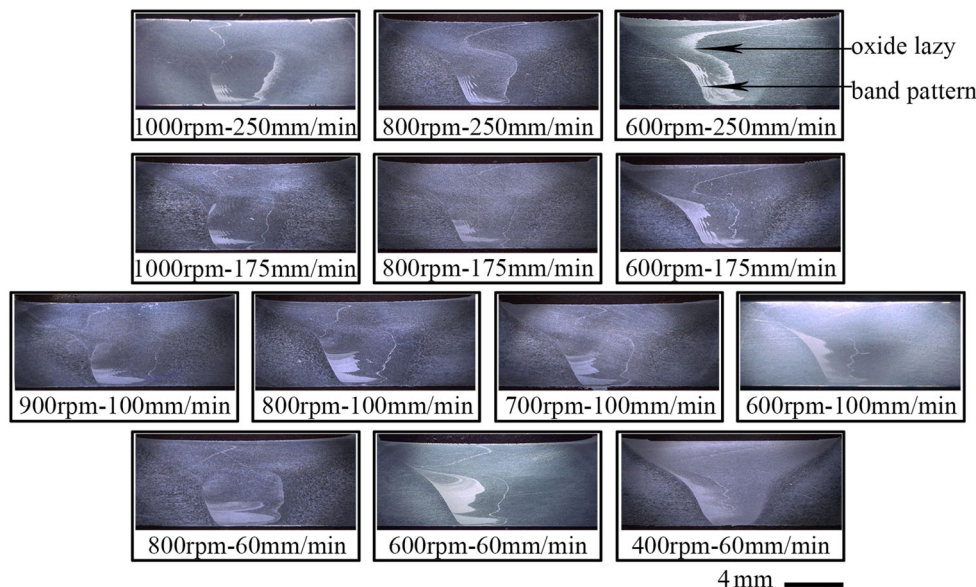


Fig. 4 Bright figures (BFs) of TEM of NZ form FSW joints under: **a** 1000 rpm–250 mm/min; **b** 600 rpm–250 mm/min; **c** 600 rpm–175 mm/min; **d** 900 rpm–100 mm/min; **e** 600 rpm–100 mm/min; **f** 800 rpm–60 mm/min

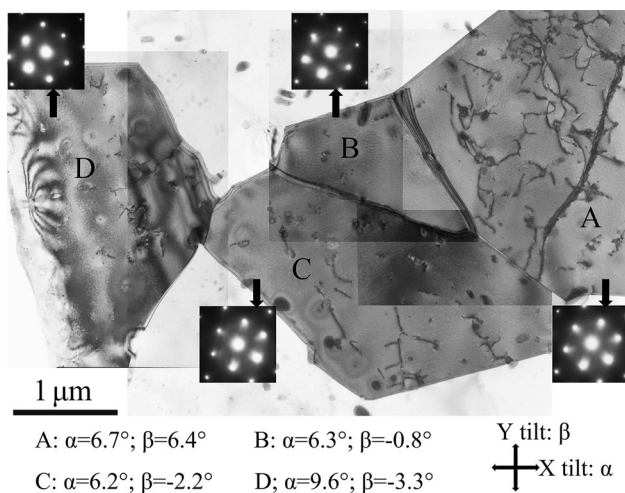
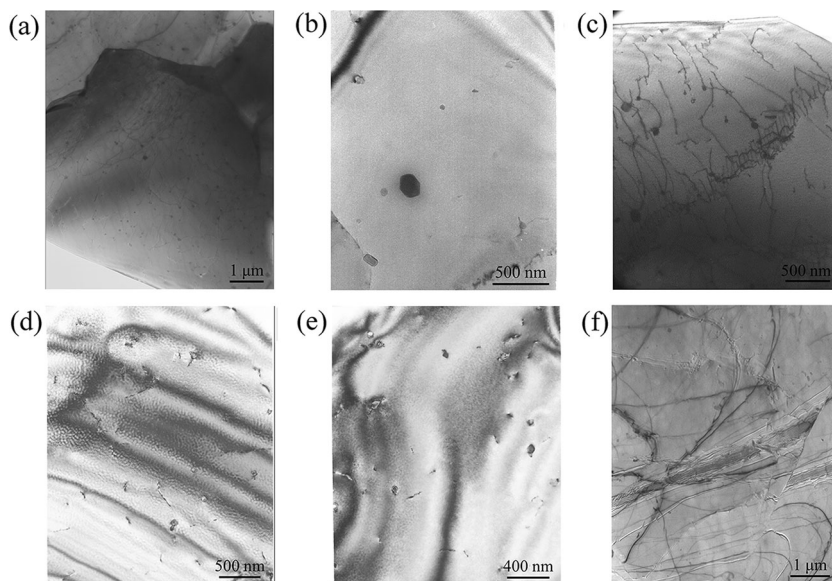


Fig. 5 BFs of adjacent grains with similar tilt angles in the NZ under 600 rpm–100 mm/min

grain boundary misorientation θ in uniformly deformed grains during CDRX was proposed by Pantleon [27]:

$$\theta = \sqrt{\gamma b/d} \quad (4)$$

where b is the burger's vector, d is the grain size, and γ is the shear strain. In addition, according to Orowan's theoretical calculation [28], it is found that the shear stress increment of dislocation line motion changes with the size of the second-phase particle spacing. In the process of CDRX, the migration of subgrain boundary is limited by the pinning effect of fine dispersed second phase. Finally, grain B is formed by absorbing the dislocations, namely the

result of CDRX, resulting from a low precipitate density. The low misorientation (1.4°) between grains B and C illustrates that grain B is nucleated within grain C. Before that, grains A and C are generated from a larger elongated grain by insufficient GDRX. A sustained deformation will bring GDRX one after another, which would further widen the misorientation between grains A and C in the future and lead to the formation of high-angle grain boundary (HAGB) [24]. The orientation of grain D can be obtained through rotating grain C around $[110]_{Al}$ incident axis by 77.3° and thus close to a $70.5^\circ \langle 110 \rangle$ twin relationship. It can be inferred as a compensatory movement of grain D in the direction perpendicular to length direction of grains A, B and C during GDRX [29–31].

4 Discussions

From a statistical standpoint, GOS maps were used to evaluate recrystallization extent. The grains recrystallized were determined by the GOS analysis within 3° [32], which located in blue area according to the colorful bar in Fig. 6. Meanwhile, the orientation spread within a grain which is fully recovered stays near 6° . Although HAGBs can be formed by GDRX, there exists a large area where dislocation density is high within the grain for the NZ under high feeding speed (250 mm/min) shown in Fig. 7a–c. The reason why the area fraction of fully recrystallization grain is low is that the ability of CDRX is limited due to low heat input under high feeding speed. Normally, reducing the feeding speed will increase the welding heat input and then reduce the resistance of GDRX and CDRX simultaneously.

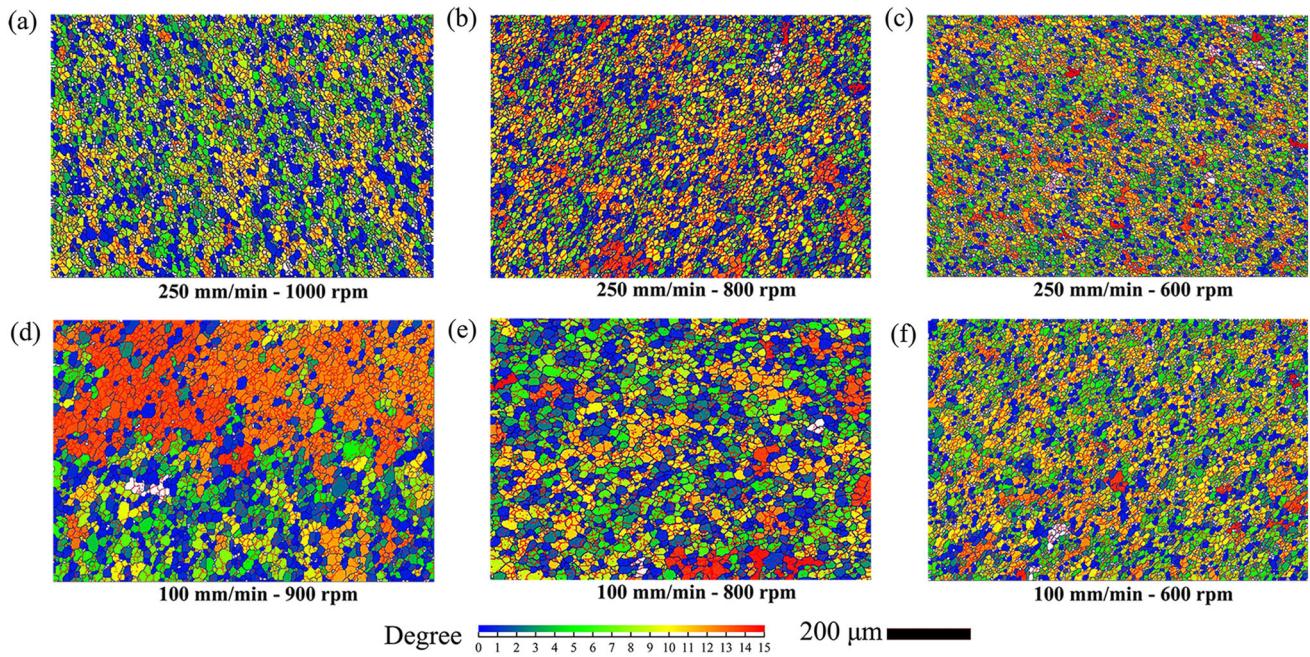


Fig. 6 Grain orientation spread (GOS) figures of the center area in NZ under different welding parameters, small angle grain boundaries ($2^\circ \sim 15^\circ$) marked as red lines and high-angle grain boundaries ($> 15^\circ$) marked as black line

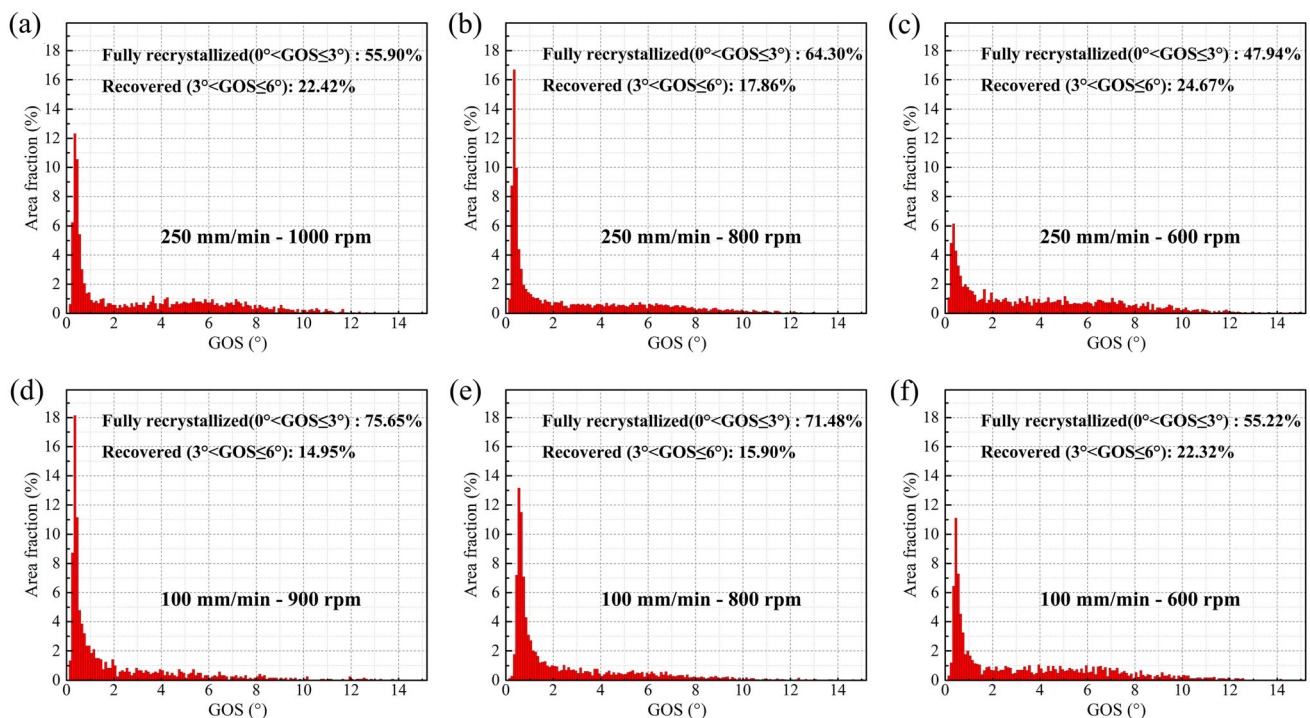


Fig. 7 The GOS distribution plots of the center area in NZ under different welding parameters

Seen from Fig. 7d–f, more and more recovered grains transform to fully recrystallization state under the influence of CDRX.

The interesting thing is that, when the feeding speed is high, the fraction of LAGBs varies nonlinearly while decreasing the rotation speed of the welding tool. However, when the feeding speed is low, the fraction of LAGBs

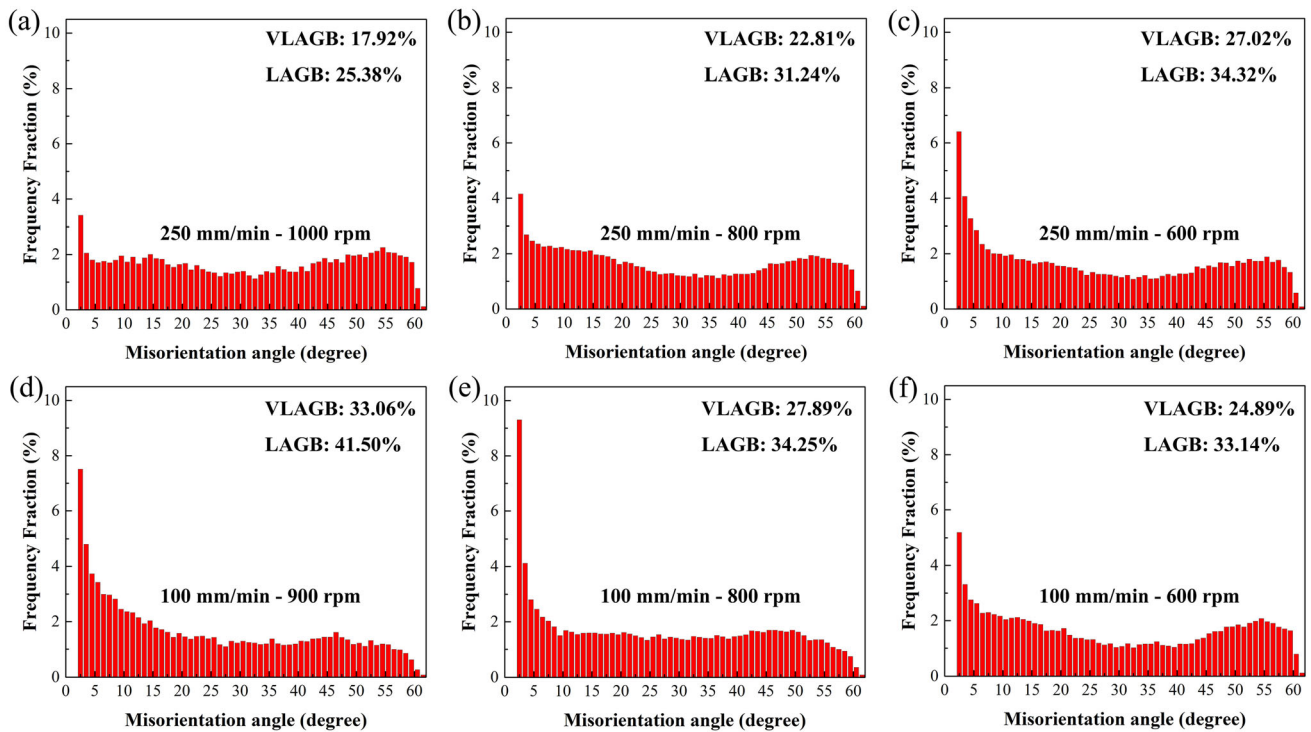


Fig. 8 The distribution of misorientation angle of GBs of the center area in NZ under different welding parameters

becomes larger while increasing the rotation speed, shown in Fig. 8. Normally, heat is generated by friction between the tool and work piece and via plastic deformation during FSW [33]. The calculated line heat input generated by friction between the tool and work piece decreases with rotation speed increasing, when maintaining a constant feeding speed shown in Fig. 9; on the contrary, for mid-thickness Al alloy (6 mm), the line heat input generated via plastic deformation will increase with the increase in rotation speed [34].

It can be inferred that maintaining a low feeding speed, as the rotation speed increases, the total heat input and the

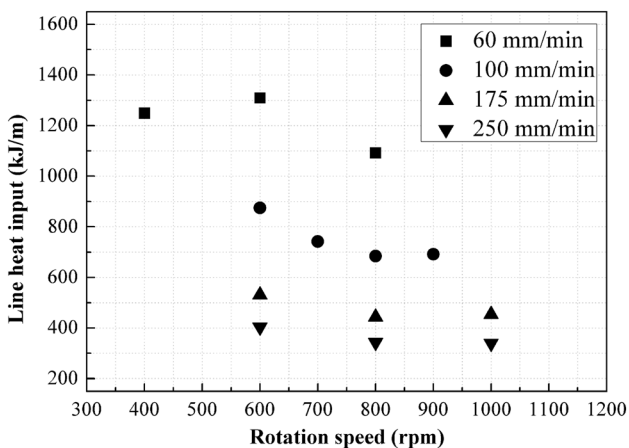


Fig. 9 Line heat input generated by friction between the tool and work piece using different welding parameters

ratio of heat via plastic deformation to heat by friction both become large. Then, a large quantity of dislocation is formed during plastic deformation and more LAGBs are formed by dynamic recovery (Fig. 8d–f); on the other hand, the high heat input generated via plastic deformation drive more grains into fully recrystallization state, compared between Fig. 7d–f. Maintaining a high feeding speed, the ratio of heat via plastic deformation to heat by friction becomes large as the rotation speed increases; meanwhile, the total heat input may be nearly the same. Thus, in this situation, a large quantity of dislocations formed during plastic deformation cannot be fully recovered under high rotation speed and a high fraction of HAGB is obtained by GDRX; but the total heat input can recover a low density of dislocation sufficiently brought by low rotation speed and then result in a high fraction of LAGB.

As mentioned before, the driving force of CDRX is the deformation storage energy which has not been released after recovery. Normally, KAM results cannot act as the criterion of static recrystallization. However, we can still find some relationship between GOS and KAM results. When different samples are compared under a constant feeding speed, the order of magnitude of average local misorientation is 100 mm/min–600 rpm > 100 mm/min–800 rpm \approx 100 mm/min–900 rpm and 250 mm/min–600 rpm > 250 mm/min–1000 rpm > 250 mm/min–800 rpm (Fig. 10). The order of magnitude of fully

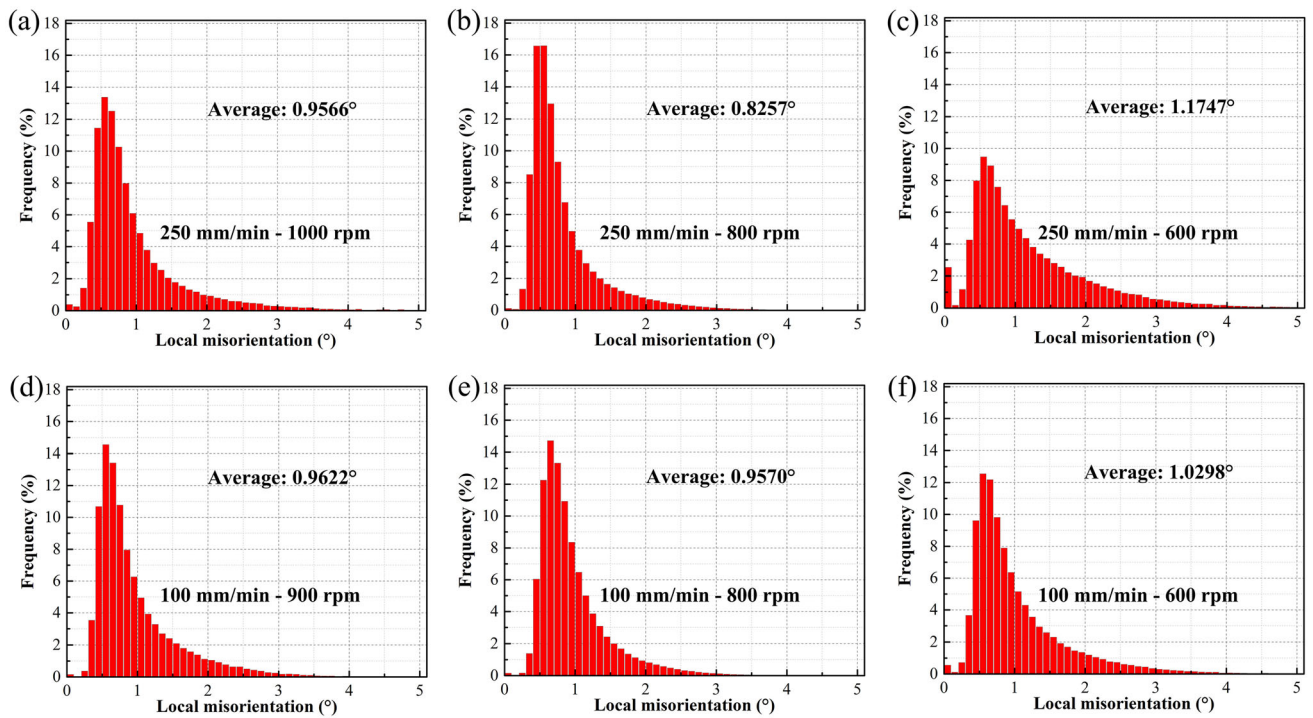


Fig. 10 Local misorientation of the center area in NZ under different welding parameters

recrystallization fraction resembles that of average local misorientation. It is obvious that KAM results can indicate extent of dynamic recrystallization in the NZ of FSW when compared under a constant feeding speed, which can be seen directly within Fig. 11a–c or with Fig. 11d–f.

As there must exist an interaction between dislocation movement during dynamic recovery and CDRX in NZ, the specific type, size and distribution of precipitates have been analyzed. One round-shaped particles in NZ are marked by circle in Fig. 12a, b, which is confirmed as overaged precipitate β -Mg₂Si. It is obvious that the diameter is normally

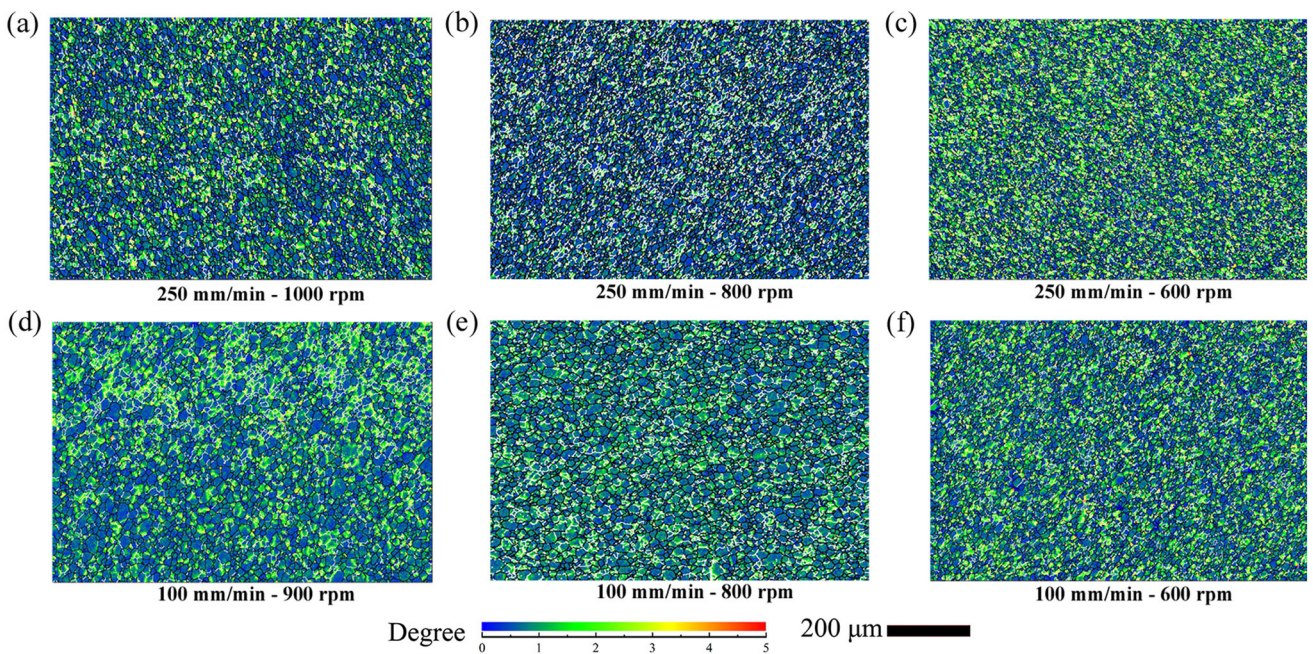


Fig. 11 KAM images of the center area in NZ under different welding parameters

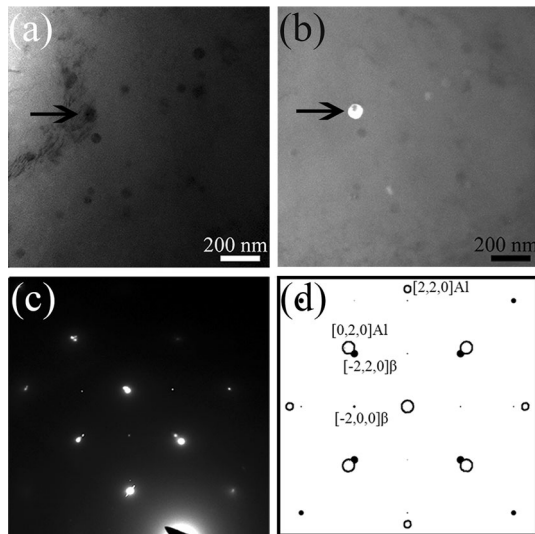


Fig. 12 TEM images of the NZ with 600 rpm rotation speed and 250 mm/min feeding speed: **a** bright field image; **b** dark field image; **c** SADP; **d** simulated SADP of the β phase under $[001]_{\text{Al}}$ zone axis indicated by solid points with the Al matrix indicated by hollow circles

smaller than 100 nm at high feeding speed. Its orientation is $[001]_{\text{Al}} // [001]_{\beta}$ and $[100]_{\text{Al}} // [110]_{\beta}$ mentioned as

conventional cube-shaped phase observed in $[001]_{\text{Al}}$ [35, 36]. Figure 13a illustrates another orientation between irregular block-shaped β phase and Al matrix, namely $(111)_{\text{Al}} // (111)_{\beta}$ and $[110]_{\text{Al}} // [110]_{\beta}$. As seen in Fig. 13b, the real multi-diffraction pattern of β phase can be verified by its corresponding single diffraction pattern shown in Fig. 13c. The irregular shape of β phase here is different from the classic hexagonal one in Al–Mg–Si–Cu alloy [37]. It can be also observed that β' phase exists in NZ regardless of feeding speed. The corresponding orientation of β' phase in Fig. 14 with Al matrix can be described as: $(001)_{\beta'} // (001)_{\text{Al}}$, $[110]_{\beta'} // [310]_{\text{Al}}$ and $[100]_{\beta'} \wedge [100]_{\text{Al}} \approx 11^\circ$. The orientation of Fig. 15 is $(001)_{\beta'} // (001)_{\text{Al}}$, $[1-10]_{\text{Al}} // [1-30]_{\beta'}$ and $[100]_{\text{Al}} \wedge [100]_{\beta'} \approx 0^\circ$. So, the low FSW feeding speed, namely enhanced dynamic recovery and CDRX, also alter the orientation of precipitates.

Previous research [38–41] has shown that the orientation alteration of precipitates can be caused by changing the interface energy with Al matrix, such as interface segregation of heavy metal atoms (Cu and Ag, etc.), dislocations and stress field. The heat input will increase when the feeding speed decreases. In this situation, the diffusion of atoms get accelerated. Then, Cu atoms are attached to the interface between Al and precipitate (β' phase or β phase, etc.). Besides, the CDRX in NZ also means a large quantity

Fig. 13 TEM images of the NZ with 600 rpm rotation speed and 60 mm/min feeding speed: **a** BF; **b** SADP; **c** simulated SADP of β phase under $[110]_{\text{Al}}$ zone axis indicated by solid points with Al matrix indicated by hollow circles

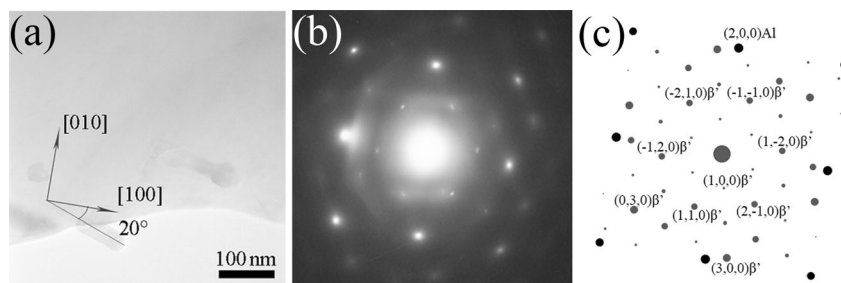
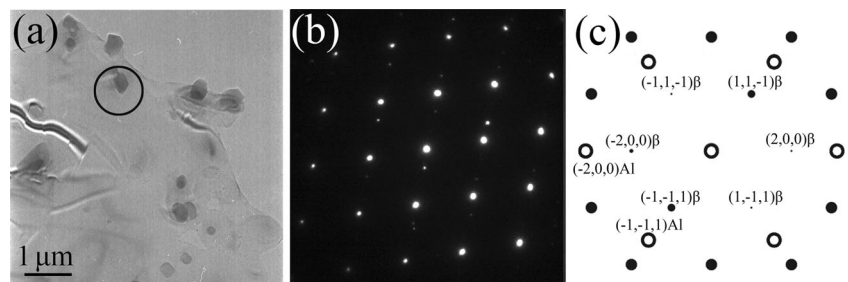
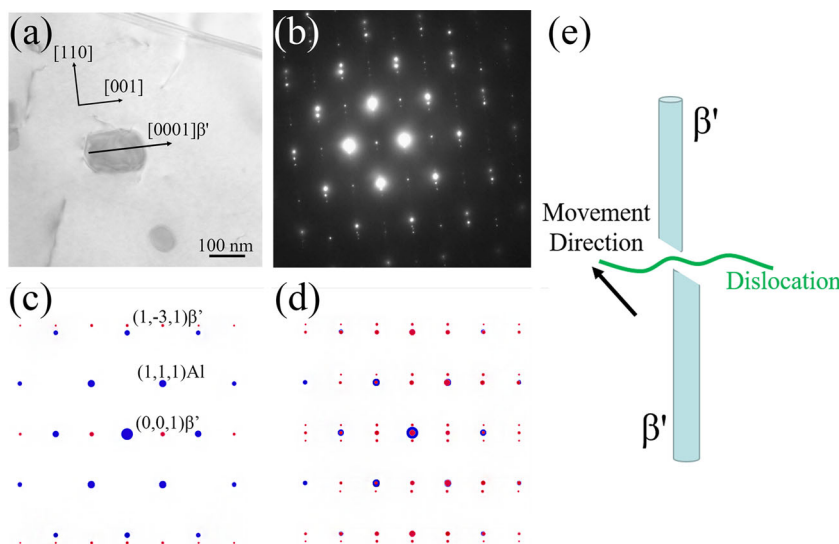


Fig. 14 TEM images of the NZ with 600 rpm rotation speed and 250 mm/min feeding speed: **a** bright-field image; **b** electron diffraction patterns from selected zone; **c** simulated SADP of the β' phase under $[001]_{\text{Al}}$ zone axis indicated by black solid points with the Al matrix indicated by grey points

Fig. 15 TEM images of the NZ with 400 rpm rotation speed and 60 mm/min feeding speed: **a** BF; **b** SADP; **c** simulated SADP of β' phase under $[110]_{Al}$ zone axis indicated by red solid points with Al matrix indicated by blue solid circles; **d** double diffraction of β'



of dislocation movements. When the dislocations pass the precipitates, the interface energy also can be affected. The bright figure in Fig. 14 is the cross section of β' phase. Fortunately, the β' phase is observed in direction perpendicular to its $[001]$ c axis (β' phase's length direction) in Fig. 15. It is clearly shown that the dimension of originally rod-shaped β' phase's length direction is largely decreased which gives a delusion that this may be a β phase, and dislocations exist near the β' phase. Although the breakdown of inter granular precipitate has also been reported to be equiaxed in the NZ grains of AA6101-T6 and AA6351-T6 [42], the type should be β phase as mentioned in these literatures. Thus, in this paper, there is a strong possibility

that deformation caused by the pin during FSW has broken down the β' phase from inside the grain.

All the tensile samples of the joints under different welding parameters fracture in the heat-affected-zone with ductile morphologies. It means the dynamic recrystallization has prevented NZ from becoming the vulnerable segment in the AA6061-T6 FSW joint. Among these parameters, a high feeding speed with a moderate rotation speed, such as 250 mm/min–800 rpm, shows better mechanical properties, shown in Fig. 16.

5 Conclusions

This paper studied the NZ of FSW joint of AA6061-T6 by EBSD. Grain orientation spread (GOS) results, kernel average misorientation (KAM) results, misorientation maps of GBs and selected area diffraction patterns of precipitate were obtained. Based on the results and analysis, the following conclusion can be drawn:

1. For 6061 Al alloy, the NZ contains fully recrystallization grains and also grains with a large density of dislocations. CDRX and GDRX both have occurred. The area fraction of recovered grains and fully recrystallization grains will increase by enhanced dynamic recovery and CDRX, when decreasing feeding speed of FSW.
2. The fraction of LAGB, recovered grains and fully recrystallization grains both increase by increasing

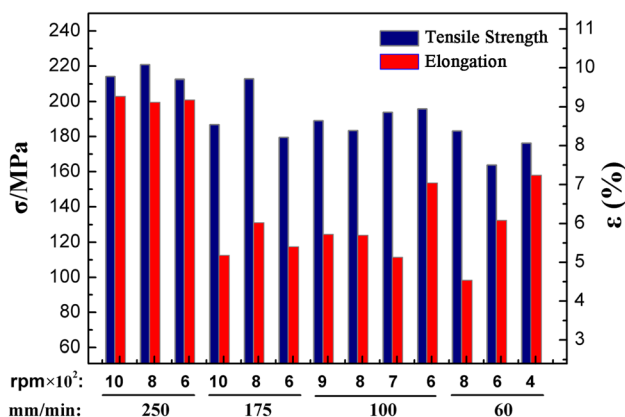


Fig. 16 The tensile properties of FSW joints of 6061-T6

rotation speed of FSW when maintaining a constant low feeding speed, which is caused by severe plastic deformation and its driving force. The opposite trend of fraction of LAGB under high feeding speed has been found, which is inferred that ratio of heat via plastic deformation to heat by friction and the total heat input may be another situation by changing rotation speed; namely, besides CDRX, the effect of GDRX is also obvious by increasing rotation speed while maintaining a high feeding speed.

3. KAM results can indicate extent of dynamic recrystallization in the NZ of FSW, only compared between different rotation speed under a constant feeding speed.
4. The high density of fine needle-shaped β'' precipitate is the main strengthening source for AA6061-T6, which disappears and evolves to β' and equilibrium β -Mg₂Si phase during FSW. Furthermore, since CDRX is accelerated by consuming the dislocation, the shape and orientation of β' or β phases can be changed by mutual interaction with dislocation movement, to different extent depending on CDRX.

Acknowledgements This project is supported by 2018 Key Research and Development Project of Shandong Province (No.2018CXGC0403).

Data availability The raw/processed data required to reproduce these findings cannot be shared at this time due to technical or time limitations.

References

1. Ramesh P N, Suwas S, Kumar K S, Sinha P P and Ranganathan S 2012 *Mater Sci Forum* **702** 315 doi: <https://doi.org/10.4028/www.scientific.net/MSF.702-703.315>
2. Lopez-Pedrosa M, Wynne B P and Rainforth W M 2007 *Mater Sci Forum* **550** 223 doi: <https://doi.org/10.4028/www.scientific.net/MSF.550.223>
3. Hadadzadeh A, Mokdad F, Wells M A and Chen D L 2018 *Mat Sci Eng A* **709** 285 doi: <https://doi.org/10.1016/j.msea.2017.10.062>
4. Zhao K, Gao T, Yang H, Liu G, Sun Q, Wu C, Nie J and Liu X 2020 *J Alloy Compd* **820** 153089 doi: <https://doi.org/10.1016/j.jallcom.2019.153089>
5. Mishra R S and Ma Z Y, 2005 *Mat Sci Eng R* **50** 1 doi: <https://doi.org/10.1016/j.mser.2005.07.001>
6. Nandan R, DebRoy T and Bhadeshia H K D H 2008 *Prog Mater Sci* **53** 980 doi: <https://doi.org/10.1016/j.pmatsci.2008.05.001>
7. Chang C I, Du X H and Huang J C 2008 *Scripta Mater* **59** 356 doi: <https://doi.org/10.1016/j.scriptamat.2008.04.003>
8. Etter A L, Baudin T, Fredj N and Penelle R 2007 *Mat Sci Eng A* **445** 94 doi: <https://doi.org/10.1016/j.msea.2006.09.036>
9. Kumar P and Sharma S 2021 *Trans Indian Inst Met* **74** 1943 doi: <https://doi.org/10.1007/s12666-021-02255-0>
10. Vahdati M, Moradi M and Shamsborhan M 2020 *Trans Indian Inst Met* **73** 2587 doi: <https://doi.org/10.1007/s12666-020-02075-8>
11. Bisadi H, Rasaee S and Farahmand M 2014 *Trans Indian Inst Met* **67** 989 doi: <https://doi.org/10.1007/s12666-014-0421-8>
12. Thilagham K T and Muthukumar S 2020 *Trans Indian Inst Met* **73** 2415 doi: <https://doi.org/10.1007/s12666-020-02063-y>
13. Subbaiah K, Geetha M, Govindaraju M and Rao S R K 2012 *Trans Indian Inst Met* **65** 155 doi: <https://doi.org/10.1007/s12666-011-0117-2>
14. Thilagham K T, Sunilkumar D and Muthukumar S 2021 *Trans Indian Inst Met* **74** 331 doi: <https://doi.org/10.1007/s12666-020-02126-0>
15. Cheong S and Weiland H 2007 *Mater Sci Forum* **558** 153 doi: <https://doi.org/10.4028/www.scientific.net/MSF.558-559.153>
16. Jata K V and Semiatin S L 2000 *Scripta Mater* **43** 743 doi: [https://doi.org/10.1016/s1359-6462\(00\)00480-2](https://doi.org/10.1016/s1359-6462(00)00480-2)
17. Rhodes C G, Mahoney M W, Bingel W H, Spurling R A and Bampton C C 1997 *Scripta Mater* **36** 69 doi: [https://doi.org/10.1016/s1359-6462\(96\)00344-2](https://doi.org/10.1016/s1359-6462(96)00344-2)
18. Su J Q, Nelson T W, Mishra R and Mahoney M 2003 *Acta Mater* **51** 713 doi: [https://doi.org/10.1016/s1359-6454\(02\)00449-4](https://doi.org/10.1016/s1359-6454(02)00449-4)
19. Zuo J, Hou L, Shi J, Cui H, Zhuang L and Zhang J 2017 *Mater Charact* **130** 123 doi: <https://doi.org/10.1016/j.matchar.2017.05.038>
20. Jazaeri H and Humphreys F J 2004 *Acta Mater* **52** 3239 doi: <https://doi.org/10.1016/j.actamat.2004.03.030>
21. Schuh C A, Kumar M and King W E 2005 *J Mater Sci* **40** 847 doi: <https://doi.org/10.1007/s10853-005-6500-9>
22. Kumar M, Schwartz A J and King W E 2002 *Acta Mater* **50** 2599 doi: [https://doi.org/10.1016/s1359-6454\(02\)00090-3](https://doi.org/10.1016/s1359-6454(02)00090-3)
23. Wang T, Zou Y, Liu X and Matsuda K 2016 *Mat Sci Eng A* **671** 7 doi: <https://doi.org/10.1016/j.msea.2016.06.050>
24. Prangnell P B and Heason C P 2005 *Acta Mater* **53** 3179 doi: <https://doi.org/10.1016/j.actamat.2005.03.044>
25. Darbal A D, Ganesh K J, Liu X, Lee S B, Ledonne J, Sun T, Yao B, Warren A P, Rohrer G S, Rollett A D, Ferreira P J, Coffey K R and Barmak K 2013 *Microsc Microanal* **19** 111 doi: <https://doi.org/10.1017/s1431927612014055>
26. Chan H M and Humphreys F J 1984 *Acta Metall* **32** 235 doi: [https://doi.org/10.1016/0001-6160\(84\)90052-x](https://doi.org/10.1016/0001-6160(84)90052-x)
27. Pantleon W 1998 *Acta Mater* **46** 451 doi: [https://doi.org/10.1016/s1359-6454\(97\)00286-3](https://doi.org/10.1016/s1359-6454(97)00286-3)
28. Orowan E 1934 *Zeitschrift Fur Physik* **89** 605 doi: <https://doi.org/10.1007/bf01341478>
29. Fullman R L and Fisher J C 1951 *J Appl Phys* **22** 1350 doi: <https://doi.org/10.1063/1.1699865>
30. Gleiter H 1969 *Acta Metall* **17** 1421 doi: [https://doi.org/10.1016/0001-6160\(69\)90004-2](https://doi.org/10.1016/0001-6160(69)90004-2)
31. Yang P and Engler O 1998 *Mater Charact* **41** 165 doi: [https://doi.org/10.1016/S1044-5803\(98\)00027-8](https://doi.org/10.1016/S1044-5803(98)00027-8)
32. Alvi M H, Cheong S, Weiland H and Rollett A D 2004 *Mater Sci Forum* **467** 357 doi: <https://doi.org/10.4028/www.scientific.net/MSF.467-470.357>
33. Su H, Wu C S, Bachmann M and Rethmeier M 2015 *Mater Design* **77** 114 doi: <https://doi.org/10.1016/j.matdes.2015.04.012>
34. Su H, Wu C S, Pittner A and Rethmeier M 2014 *Energy* **77** 720 doi: <https://doi.org/10.1016/j.energy.2014.09.045>
35. Matsuda K, Ishida Y, Mullerova I, Frank L and Ikeno S 2006 *J Mater Sci* **41** 2605 doi: <https://doi.org/10.1007/s10853-006-7819-6>
36. Matsuda K, Kawabata T, Uetani Y, Sato T and Ikeno S 2002 *J Mater Sci* **37** 3369 doi: <https://doi.org/10.1023/a:1016545124410>
37. Matsuda K, Kawabata T, Uetani Y, Sato T and Ikeno S 2002 *Scripta Mater* **47** 467 doi: [https://doi.org/10.1016/s1359-6462\(02\)00173-2](https://doi.org/10.1016/s1359-6462(02)00173-2)
38. Fiawoo M, Gao X, Bourgeois L, Parson N, Zhang X Q, Couper M and Nie J F 2014 *Scripta Mater* **88** 53 doi: <https://doi.org/10.1016/j.scriptamat.2014.05.013>

39. Matsuda K, Uetani Y, Sato T and Ikeno S 2001 *Metall Mater Trans A* **32** 1293 doi: <https://doi.org/10.1007/s11661-001-0219-2>
40. Cayron C and Buffat P A 2000 *Acta Mater* **48** 2639 doi: [https://doi.org/10.1016/s1359-6454\(00\)00057-4](https://doi.org/10.1016/s1359-6454(00)00057-4)
41. Yassar R S, Baird J C and Horstemeyer M F 2009 *Mat Sci Eng A* **517** 286 doi: <https://doi.org/10.1016/j.msea.2009.04.013>
42. Das U, Toppo V, Sahoo T K and Sahoo R 2018 *Trans Indian Inst Met* **71** 823 doi: <https://doi.org/10.1007/s12666-017-1213-8>

Publisher's Note Springer Nature remains neutral with regard to jurisdictional claims in published maps and institutional affiliations.